Diamond & Related Materials 116 (2021) 108403

Contents lists available at ScienceDirect

Diamond & Related Materials

journal homepage: www.elsevier.com/locate/diamond

Temperature dependence of Young's modulus of single-crystal diamond determined by dynamic resonance

Xiulin Shen [a,b], Kongping Wu [d], Huanying Sun [a], Liwen Sang [c], Zhaohui Huang [b,*], Masataka Imura [a], Yasuo Koide [a], Satoshi Koizumi [a], Meiyong Liao [a,*]

[a] Research Center for Functional Materials, National Institute for Materials Science, Namiki 1-1, Tsukuba, Ibaraki 305-0044, Japan
[b] School of Materials Science and Technology, China University of Geosciences (Beijing), Beijing 100083, China
[c] International Center for Materials Nanoarchitectonics (MANA), National Institute for Materials Science (NIMS), Namiki 1-1, Tsukuba, Ibaraki 305-0044, Japan
[d] School of Electronics and Information Engineering, Jinling Institute of Technology, Nanjing, Jiangsu 211169, China

ARTICLE INFO

Keywords:
Single crystal diamond
Young's modulus
High temperature
Mechanical resonance

ABSTRACT

Young's modulus is a key parameter for mechanical engineering and always performs a significant role in materials design. Diamond has been regarded as an ideal material for MEMS devices and can be used in complex environments, which requires a quantitative and accurate measurement of the Young's modulus. However, as a material with outstanding mechanical rigidity and chemical inertness, the wide temperature dependent Young's modulus of single-crystal diamond (SCD) is rarely reported. In this paper, the Young's modulus of (100) oriented SCD from room temperature to 700 °C is determined experimentally and theoretically by dynamic resonance frequency method based on SCD MEMS cantilevers and first-principles calculation. The dependence of the Young's modulus of SCD is obtained by the resonance frequencies shift of the SCD cantilevers. The results show that despite different residual stress in each measured cantilever, the Young's modulus of SCD *versus* temperature obeys the same model as temperature increases from room temperature to 700 °C, consistent with the results calculated from the first-principles calculation. This research proposes a convenient and accurate method to measure the dependence of SCD Young's modulus on temperature, which provides a valuable reference for the advanced development of SCD MEMS and other mechanical applications.

1. Introduction

Young's modulus (E_Y) is a fundamental key physical quantity for mechanical fabrication, especially of great sense for the design and assessment of nano/micro-electromechanical systems (NEMS/MEMS) [1]. Single-crystal diamond (SCD) is an ideal material for advanced MEMS applications due to the highest mechanical hardness and highest Young's modulus known in nature [2–4]. Besides, owing to the complex environmental conditions for using MEMS devices, SCD has great potential for applications benefitting from its outstanding thermal conductivity, electronic properties, and chemical inertness [5–7]. As a basic parameter for the applications for electromechanical or thermo-mechanical devices, *i.e.*, MEMS sensors under high temperatures [8–10] and thermal probes in a scanning microscopy [11–13], it is necessary to accurately determine the Young's modulus of SCD at room temperature (RT) and its dynamic dependence on wide temperature change.

Numerous researchers have reported different methods to measure and evaluate the Young's modulus of different materials [14–17], especially the traditional materials such as silicon [18–20], which is widely used for conventional MEMS fabrication. Table 1 lists some typical methods for diamond Young's modulus measurement at RT. Although each method has its own advantages, the dynamic resonance frequency method based on MEMS resonators is considered to be the most practical one with outstanding accuracy [20,21] due to the high sensitivity and batch production of MEMS resonators.

There are several reports on the Young's modulus of diamond. Klein et al. [30] evaluated the Young's modulus by means of bulge testing at room temperature, in which the deflection of a large-diameter thin membrane was measured under pressures. McSkimin et al. [23] obtained variations of diamond wave velocities and moduli over a temperature range from +50 °C to −195.8 °C by refined ultrasonic experiments. Adiga et al. [31] showed that the ultrananocrystalline diamond Young's modulus increased 3.1% as temperature reduced from 300 K to 138 K by resonant frequency measurement on Si-based

* Corresponding author.
E-mail addresses: huang118@cugb.edu.cn (Z. Huang), meiyong.liao@nims.go.jp (M. Liao).

https://doi.org/10.1016/j.diamond.2021.108403
Received 17 January 2021; Received in revised form 29 March 2021; Accepted 6 April 2021
Available online 19 April 2021

Table 1
Methods for diamond E_Y measurement.

Methods	Measured parameters	Pros and cons	References
Ultrasonics with acoustic waves	Sound velocity	Easy operation; difficult for ultrathin or complex shapes of samples;	Ref. [22, 23]
Brillouin scattering	Frequency shifts of Brillouin components	Accurate; convenient for comprehensive measurement; small frequency shift and weak scattering intensity;	Ref. [24–26]
Nanoindentation	Load-deflection curve	Simple; inaccurate;	Ref. [27, 28]
Resonant frequency	Mechanical resonance frequencies	Convenient; no damage;	Ref. [29]

structure cantilevers. Maribel et al. [32] computed the elasticity of diamond at high pressures and temperatures in the ranges of 0–500 GPa and 0–4800 K using first-principles calculation. However, there are few experimental reports on SCD Young's modulus at high temperatures above RT.

Here, in order to accurately evaluate the (100) oriented SCD Young's modulus at RT and its dependence on temperature, we developed the SCD-on-SCD micro-cantilevers based on the smart-cut method and monitored the resonance frequency shifts of the cantilevers as temperature increased from RT to 700 °C. Besides, first-principles calculation (FPC) was performed to verify the credibility of the experimental results. It was shown that the Young's modulus of the SCD cantilevers decreased with increasing temperature but the change was small. Despite different residual stress in each measured cantilever, the Young's modulus of SCD followed the same model with temperature.

2. Experimental methods

The SCD-on-SCD micro-cantilevers in this work were fabricated by ion-implantation assisted smart-cut method [33,34]. In this method, a graphite-like sacrificial layer was embedded in the SCD substrate by high-energy ion implantation. With the removal of the sacrificial layer by photolithography, reactive ion etching, and wet-etching, the SCD cantilevers were released. The smart-cut method has the advantages of controlled dimensions from nanoscale to microscale, and high reproducibility in the fabrication process of cantilevers. More details are described in the Supplementary Information. The fabricated cantilevers were divided into two sets: set-I and set-II. Both the two sets of cantilevers were fabricated by the same method but with different thicknesses. Set-I cantilevers were broken to measure the thickness by 3D laser optical microscope and for the calculation of Young's modulus of SCD at room temperature, and set-II cantilevers were used to study the relationship between Young's modulus and temperature. It is worth mentioning that during the MPCVD growth with the substrate temperature >900 °C, the annealing of SCD was actually conducted at the same time, which eliminated the majority of defects caused by ion implantation and recovered the elastic modulus of SCD [35]. Besides, the fabricated cantilevers were annealed at 700 °C for 3 h in the measurement vacuum chamber to reduce the effect of the surface absorption on the resonance frequency and Q factor. Fig. 1(a–b) shows the 3D optical images of the two as-prepared cantilever groups. The resonance frequencies were measured by using a laser Doppler vibrometer in a high-vacuum (10^{-3} Pa) chamber to minimize the air damping effect. A Lake Shore Model 335 temperature controller was used to heat set-II cantilevers from RT to 700 °C in a step of 50 °C. The obtained resonance frequencies were fitted by the Lorentzian line shape and the quality (Q) factors were obtained by dividing the resonance frequency with the full-width at half-maximum of the Lorentzian fit [36]. To obtain the experimental Young's modulus, the thickness of the set-I SCD cantilevers was measured based on the broken ones by using the 3D laser optical microscopy, shown as Fig. 1(c), and the measured thickness is 804 (±5) nm.

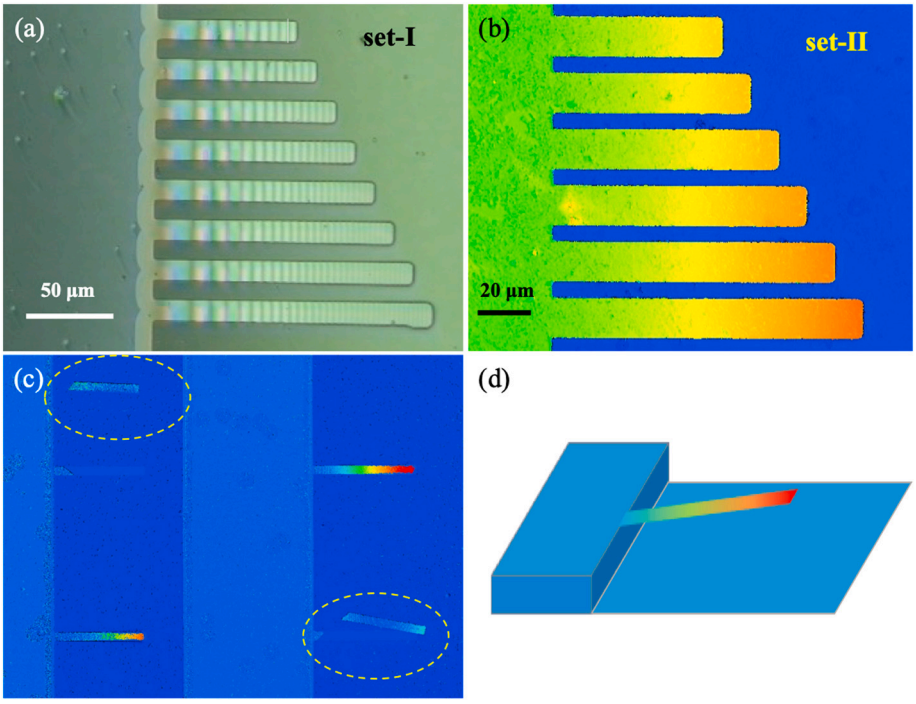

Fig. 1. The optical image of SCD cantilever arrays fabricated by the smart-cut method: (a) set-I cantilevers with length L from 70 μm to 140 μm in a step of 10 μm and width w of 12 μm; (b) set-II cantilevers with length from 90 μm to 140 μm in a step of 10 μm, width of 12 μm, and thickness t of ~1.44 μm; (c) measured thickness t of 804 (±5) nm of broken SCD cantilevers from set-I (d) the side view scheme of a cantilever.

3. Results and discussion

3.1. Determination of the Young's modulus of SCD at room temperature

We firstly estimated the Young's modulus of SCD at room temperature by measuring the length-dependent resonance frequency of the cantilevers using set-I cantilevers. As revealed in Fig. 1(a), gradient color can be seen due to different bending degree of the cantilevers, which indicates that there may still be small initial residual stress resulting from the surface imperfection. Fig. 2 shows the dependence of measured resonance frequencies f_σ on length L for set-I cantilevers, which exhibits excellent agreement with the modified Euler-Bernoulli theory [37]:

$$f_\sigma = f_0\sqrt{1+\frac{60\sigma L^2}{14E_Y t^2}} \tag{1}$$

This formula takes the residual stress σ into account for rectangular cross-section cantilever beam, and f_0 is the theoretical resonance frequency of cantilevers without considering any residual stress [38], equaling to:

$$f_0 = \frac{K^2 t}{2\pi L^2}\sqrt{\frac{E_Y}{12\rho}} \tag{2}$$

In both formulas, K is determined by the vibration mode number, E_Y is the Young's modulus, ρ is the mass density, and t is the cantilever thickness.

From the resonance frequencies of set-I cantilevers, E_Y is fitted to be around 1144.5 (±14) GPa and the residual stress σ is as small as 1.08 MPa, respectively, where E_Y is close to the results obtained by MHz-ultrasonic interferometry of 1141 (±12) GPa [22] and by Brillouin scattering of 1142.7 (±3) GPa [39,40]. The actual residual stress may have some slight differences, but the fitting curve of resonance frequencies is quite consistent with the measured f_σ. Hence, E_Y obtained based on micro-cantilever method is considered to be more reliable and practical than conventional methods. The low stress should not affect the reliability of the SCD MEMS [37,38].

3.2. Temperature dependent Young's modulus

We characterized the temperature effect on the Young's modulus up to 700 °C in a high vacuum chamber. Fig. 3(a) shows a linear dependence of measured resonance frequencies f_σ on the cantilevers length $1/L^2$ at different temperatures, exhibiting outstanding rigidity and stability even at 600 °C. Fig. 3(b) shows the dependence of the measured resonance frequencies f_σ and Q factors of the SCD cantilevers on length L at RT. The residual stress σ evaluated by Eq. (1) is also inserted, which is less than 15 MPa and has little effect on the Q factor of cantilevers. The residual stress results in an increase of the resonance frequencies, implying a tensile stress over the cantilevers [41]. The Q factors of the SCD cantilevers may be markedly enhanced under large stresses as high as GPa [42,43] and reach 1 million after atomic scale etching the bottom defects [44,45].

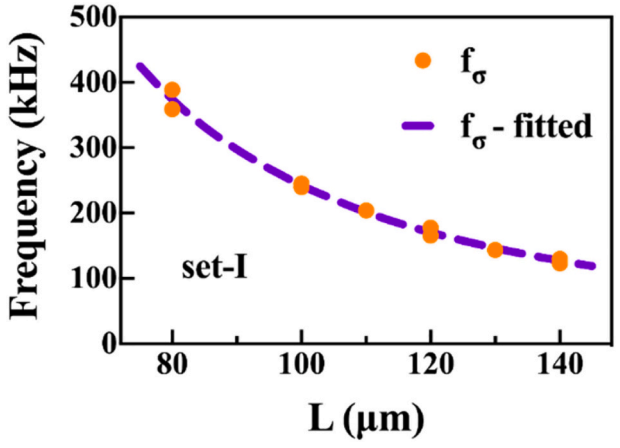

Fig. 2. Dependence of measured resonance frequencies (f_σ, orange dots) on cantilevers length at RT. The purple dashed line is the fitted data.

As the measurement temperature rises, the resonance frequencies of the cantilevers decrease. The frequency shift of a 90 μm-cantilever is illustrated in Fig. 4(a). The temperature coefficient of frequency (TCF) of the SCD cantilevers is shown in Fig. 4(b), which is as small as <6 ppm/°C below 700 °C. The small TCF further confirms the reliability of the measurement of the Young's modulus, excluding other external effect such as surface absorption effect on the frequency.

In Fig. 5, we show the measured temperature dependent resonance frequencies and Q factors of the 90 μm- and 140 μm-long cantilevers. The data of other cantilevers are described in Fig. S1, which show the same tendency as those of here. In general, the Q factors first increase and then decrease as the temperature rises to 700 °C, but always higher than 3000. The dependence of Q factors on the temperature was explained by bulk defects and thermal elastic dissipation (TED) [46]. The resonance frequencies display a downward nonlinear trend with temperature increasing, which can be attributed to the reduction of the Young's modulus of the SCD cantilever. Absolutely, the anharmonic effect of lattice vibration and the change of bond length with temperature result in the dependence of the Young's modulus of crystal materials on temperature [47]. The residual stress σ is also considered for the accurate estimation of the Young's modulus.

Considering the slope of $E_Y - T$ decreases from a constant value to zero as temperature lowers, the temperature (T) dependence of Young's modulus (E_Y) is assumed to be as follows [48]:

$$E_Y = E_0 - ATexp\left(-\frac{T_0}{T}\right), \tag{3}$$

where E_0 (GPa) is the Young's modulus at 0 K, A is a constant independent of temperature, T_0 is a characteristic parameter of diamond approximately equal to $\Theta_D/2$ [49], and T is temperature in the unit of K. The dependence of stress on temperature is assumed as Eq. (4):

$$\sigma = \sigma_0 - BTexp\left(-\frac{C}{T}\right), \tag{4}$$

where σ_0 is the stress of cantilever at 0 K, and the other two coefficients B and C are constants independent of temperature. Table 2 lists the fitted parameters for the 90 μm- and 140 μm-cantilevers. The parameters from other cantilevers are listed in Table S1, and the average values from all the cantilevers are used here.

The dependence of the fitted residual stress σ on temperature T for the SCD cantilevers is also illustrated in Fig. S2. Note that the value of σ changes little within the investigated temperature range. The calculated dependence of E_Y on temperature is shown in Fig. 6, in which the reported data in literatures are also presented [23,50,51].

The value of E_Y decreases by a factor of 0.79% in our measurement, which is close to Szuecs' linear fitting curve with temperature from RT to 700 °C (~0.89%) [50]. However, the linear fitting curve of E_Y *vs* T lacks the credibility below RT. On the other hand, the fitted E_Y *vs* T below RT in this work is close to McSkimin's experimental data [23], but slightly differs from Migliori's experimental one [51]. The error of E_Y *vs* T is as low as ~0.05% in this work and the theoretical fitting of the resonance frequencies $f_{\sigma-fitted}$ *vs* T calculated from the fitted E_Y at temperature from RT to 700 °C are comparable to those experimental f_σ values, as shown in Fig. 7(a–b). To further confirm the practicality of the E_Y *vs* T formula, other cantilevers (c–d) with different lengths and residual stress are also presented for comparison. The calculated curves still maintain a great agreement with experimental ones even with different residual stress. More fitted results can be found in Fig. S3.

First-principles calculations are also performed to investigate the

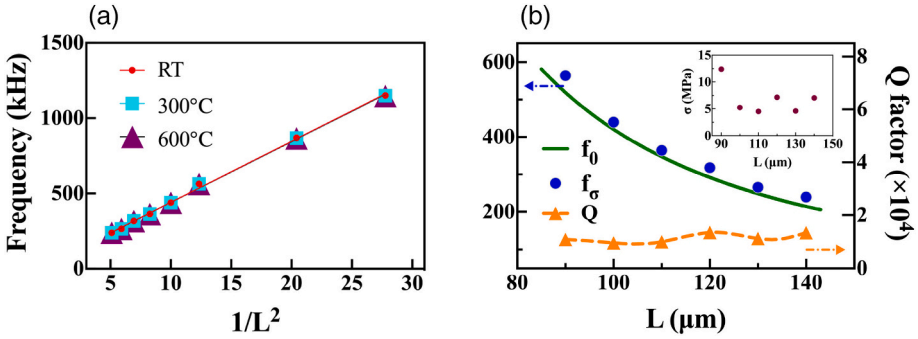

Fig. 3. (a) Dependence of the measured resonance frequencies on cantilevers length $1/L^2$ at RT, 300 °C and 600 °C, respectively; (b) dependence of the measured resonance frequencies (f_σ, blue dots), theoretical frequencies without stress (f_0, green curve), and Q factors (orange triangle) on cantilevers length L at RT. The calculated residual stress *vs* L at RT is inserted.

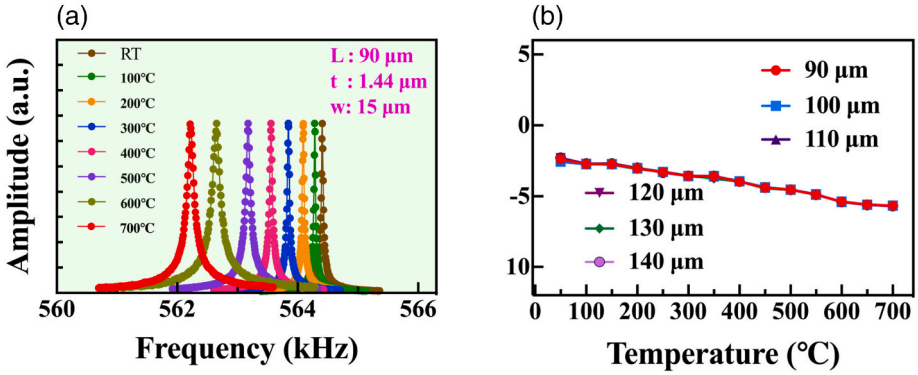

Fig. 4. (a) Resonance frequency shift of a 90 μm-cantilever on temperature increasing from RT to 700 °C; (b) temperature dependence of TCF with cantilever length varying from 90 μm to 140 μm.

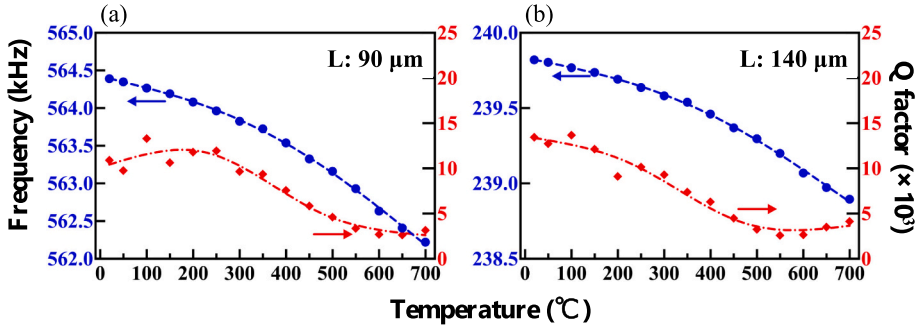

Fig. 5. Dependence of the measured cantilevers frequencies (blue circle and curve) and Q factors (red square and curve) on temperature from RT to 700 °C with length of 90 μm and 140 μm.

Table 2
Parameters obtained from fitted $f_\sigma - T$.

L	E_0 (GPa)	A (GPa/K)	T_0	σ_0 (MPa)	B (Pa)	C
90 μm	1143.23	0.03	1115.96	12.47	130.57	739.06
140 μm	1143.17	0.03	1115.97	7.07	9.23	739.35
Average[a]	1143.16	0.03	1115.97	–	–	737.49

[a] The average value is calculated from fitted parameters of cantilever length within 90 μm–140 μm as listed in Table S1.

elastic property of SCD (see Supplementary Information). For the face centered cubic diamond with Fd-3m symmetry, the three independent matrix elements are C_{11}, C_{12} and C_{44} in the elasticity tensor matrix (C_{ij}). At 0 K, the theoretical equilibrium lattice constant of diamond is 3.572 Å, which is in good agreement with the previous theoretical result [52], and is comparable to the experimental data of 3.567 Å. The calculated temperature dependence of C_{ij} are listed in Table 3, compared with other reported *ab initio* calculations [53,54] and the experimental measuring values [39].

The calculated C_{11}, C_{12} and C_{44} decrease slightly with increasing temperature (listed as Table S2 in Supplementary Information), which indicates that thermal expansion may soften the elastic modulus at higher temperatures. The deviation from experiments may be that the atomic bonding is typically underestimated in the generalized gradient approximation (GGA)-based density functional theory (DFT) computation, thereby resulting in a reduction in the elastic constants and Young's modulus. The orientation-dependent Young's modulus for ⟨100⟩ direction is calculated through the following equation [15,55]:

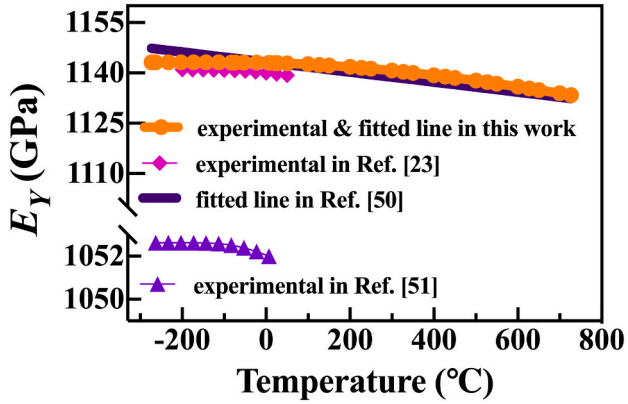

Fig. 6. Temperature dependent E_Y of SCD, including experimental data from Refs. [23] and [51], a fitted line in Ref. [50] by a linear curve $E_Y = E_{RT}[1 + c(T - 20)](c = -1.31 \times 10^{-5}\ K^{-1})$, and experimental & fitted line in this work, which can be described as $E_Y = 1143.16 - 0.03Texp\left(-\frac{1115.97}{T}\right)$.

$$E_{Y\langle 100\rangle} = \frac{(C_{11} - C_{12}) \times (C_{11} + 2 \times C_{12})}{(C_{11} + C_{12})} \quad (5)$$

To compare the FPC calculated Young's modulus with the experimental one from dynamic resonance frequencies method, we plot the normalized $E_Y(T)/E_0$ curve as a function of temperature, as presented in Fig. 8. It is revealed that the experimental E_Y *vs* T is similar to that of the theoretical one.

4. Conclusion

In conclusion, the Young's modulus of single-crystal diamond is investigated by dynamic resonance frequency method from RT to 700 °C based on SCD-on-SCD structure cantilevers. Benefitting from the extraordinary stability and accuracy of the SCD cantilevers, the dependence of single-crystal diamond Young's modulus on temperature was achieved by the resonance frequency shifts of the SCD cantilevers. The Young's modulus of all measured cantilevers obeys the same decrease tendency with increasing temperature up to 700 °C, which is proved to have excellent consistency with the one calculated from the first-principles calculation. This study of SCD Young's modulus can be used to develop SCD MEMS, especially for applications in extreme environments.

CRediT authorship contribution statement

Xiulin Shen: Methodology, Investigation, Data curation, Formal

Table 3
Calculated temperature dependence of C_{ij} and reported results for SCD.

T (K)	C_{11} (GPa)	C_{12} (GPa)	C_{44} (GPa)	
0	1050.29	123.24	560.83	This
300	1048.76	121.82	558.97	study
Ab initio[a]	1050 ± 10	127 ± 4	550 ± 5	Ref. [53]
Ab initio[a]	1043 ± 5	128 ± 5	534 ± 17	Ref. [54]
GHz-ultrasonic interferometry[a]	1074.8 ± 0.4	125.3 ± 1	575.1 ± 0.3	Ref. [39]

[a] Values obtained at room temperature.

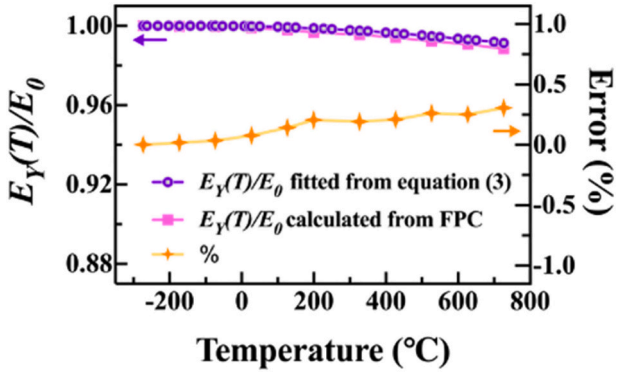

Fig. 8. Temperature dependence of $E_Y(T)/E_0$ obtained from experimental and FPC, respectively, and the error of $E_Y(T)/E_0$ between FPC and the experimental result.

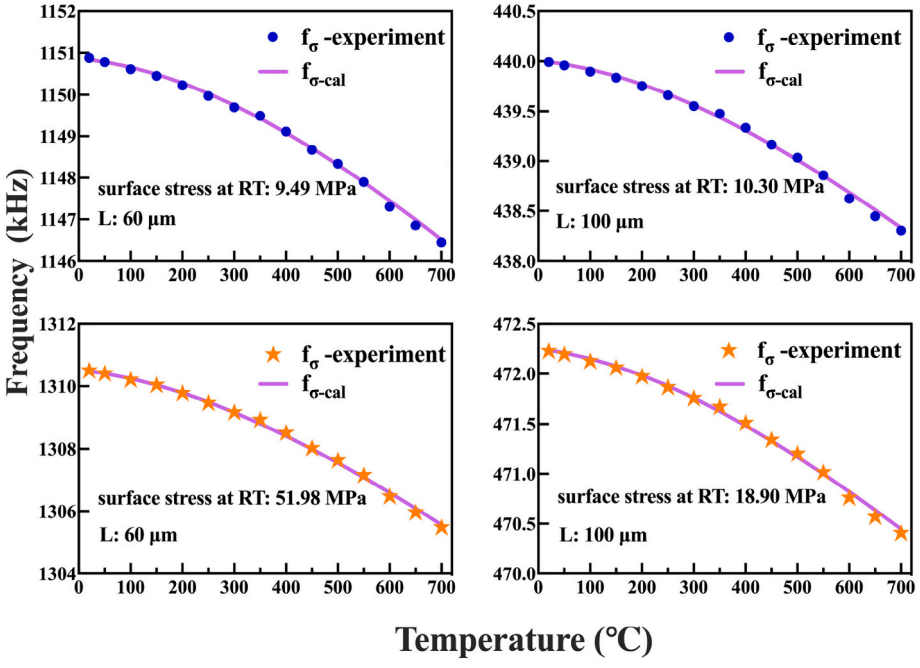

Fig. 7. Comparison between the measured frequencies (blue dots and orange stars) and those calculated from the fitted Young's modulus and stress (purple curves).

analysis, Writing-original draft. **Kongping Wu**: Methodology. **Huanying Sun**: Methodology, Validation. **Liwen Sang**: Resources, Validation. **Zhaohui Huang**: Resources, Supervision. **Masataka Imura**: Resources. **Yasuo Koide**: Resources. **Satoshi Koizumi**: Resources, Supervision. **Meiyong Liao**: Conceptualization, Validation, Writing – review & editing, Supervision.

Declaration of competing interest

The authors declare that they have no known competing financial interests or personal relationships that could have appeared to influence the work reported in this paper.

Acknowledgements

This work was partially supported by JSPS KAKENHI (Grant Number 20H02212, 15H03999, 15H03980), Tsukuba Global Innovation Promotion Agency, Science and Nanotechnology Platform projects sponsored by the Ministry of Education, Culture, Sports, Science and Technology (MEXT) of Japan. The authors also gratefully thanked the financial support from China Scholarship Council (CSC, 201906400064).

Appendix A. Supplementary data

Supplementary data to this article can be found online at https://doi.org/10.1016/j.diamond.2021.108403.

References

[1] M.A. Hopcroft, W.D. Nix, T.W. Kenny, What is the Young's modulus of silicon? J. Microelectromech. S. 19 (2) (2010) 229–238.
[2] P. Hess, The mechanical properties of various chemical vapor deposition diamond structures compared to the ideal single crystal, J. Appl. Phys. 111 (5) (2012) 3–134.
[3] A. Nagakubo, M. Arita, H. Ogi, H. Sumiya, N. Nakamura, M. Hirao, Elastic constant C_{11} of ^{12}C diamond between 10 and 613 K, Appl. Phys. Lett. 108 (22) (2016) (L430-203).
[4] A. Banerjee, D. Bernoulli, H. Zhang, M.-F. Yuen, J. Liu, J. Dong, F. Ding, J. Lu, M. Dao, W. Zhang, Ultralarge elastic deformation of nanoscale diamond, Science 360 (6386) (2018) 300–302.
[5] M. Liao, L. Sang, T. Teraji, S. Koizumi, Y. Koide, Ultrahigh performance on-chip single crystal diamond NEMS/MEMS with electrically tailored self-sensing enhancing actuation, Adv. Mater. Technol. 4 (2) (2019) 1800325.
[6] A.V. Sumant, O. Auciello, R.W. Carpick, S. Srinivasan, J.E. Butler, Ultrananocrystalline and nanocrystalline diamond thin films for MEMS/NEMS applications, MRS Bull. 35 (4) (2010) 281–288.
[7] J. Liang, Y. Nakamura, Y. Ohno, Y. Shimizu, N. Shigekawa, Room temperature direct bonding of diamond and InGaP in atmospheric air, Funct. Diamond 1 (1) (2021) 110–116.
[8] F.L. Duan, High temperature sensors for intellegent aero-engine applications, in: 33rd AIAA Aerodynamic Measurement Technology and Ground Testing Conference, 2017, p. 3239 (Denver, Colorado).
[9] P. Tanner, A. Iacopi, H.-P. Phan, S. Dimitrijev, L. Hold, K. Chaik, G. Walker, D. V. Dao, N.-T. Nguyen, Excellent rectifying properties of the n-3C-SiC/p-Si heterojunction subjected to high temperature annealing for electronics, MEMS, and LED applications, Sci. Rep. 7 (2017) 17734.
[10] X. Guo, Q. Xun, Z. Li, S. Du, Silicon carbide converters and MEMS devices for high-temperature power electronics: a critical review, Micromachines 10 (6) (2019) 406.
[11] F. Niekiel, S.M. Kraschewski, J. Müller, B. Butz, E. Spiecker, Local temperature measurement in TEM by parallel beam electron diffraction, Ultramicroscopy 176 (2017) 161–169.
[12] A. Jovic, G. Pandraud, N.S. Losilla, J. Sancho, K. Zinoviev, J.L. Rubio, E. Margallo-Ballbas, P.M. Sarro, A MEMS actuator system for an integrated 3-D optical coherent tomography scanner, J. Microelectromech. S. (2018) 259–268.
[13] S. Luo, D. Wang, J. Tang, L. Zhou, C. Duan, D. Wang, H. Liu, Y. Zhu, G. Li, H. Zhao, Circumferential-scanning endoscopic optical coherence tomography probe based on a circular array of six 2-axis MEMS mirrors, Biomed. Opt. Express 9 (5) (2018) 2104–2114.
[14] F. Ren, E.D. Case, J.R. Sootsman, M.G. Kanatzidis, H. Kong, C. Uher, E. Lara-Curzio, R.M. Trejo, The high-temperature elastic moduli of polycrystalline PbTe measured by resonant ultrasound spectroscopy, Acta Mater. 56 (20) (2008) 5954–5963.
[15] W.B. Li, K. Li, K.Q. Fan, D.X. Zhang, W.D. Wang, Temperature and pressure dependences of the elastic properties of tantalum single crystals under tensile loading: a molecular dynamics study, Nanoscale Res. Lett. 13 (1) (2018) 118.
[16] H.J. McSkimin, Measurement of elastic constants at low temperatures by means of ultrasonic waves–data for silicon and germanium single crystals, and for fused silica, J. Appl. Phys. 24 (8) (1953) 988–997.
[17] M. Fukuhara, I. Yamauchi, Temperature dependence of the elastic moduli, dilational and shear internal frictions and acoustic wave velocity for alumina, (Y) TZP and β′-sialon ceramics, J. Mater. Sci. 28 (1993) 4681–4688.
[18] E.J. Ng, V.A. Hong, Y. Yang, C.H. Ahn, C.L.M. Everhart, T.W. Kenny, Temperature dependence of the elastic constants of doped silicon, J. Microelectromech. S. 24 (3) (2015) 730–741.
[19] W. Wijaranakula, A real-time simulation of point defect reactions near the solid and melt interface of a 200 mm diameter czochralski silicon crystal, J. Electrochem. Soc. 140 (11) (1993) 3306–3316.
[20] N. Ono, K. Kitamura, K. Nakajima, Y. Shimanuki, Measurement of Young's modulus of silicon single crystal at high temperature and its dependency on boron concentration using the flexural vibration method, Jpn. J. Appl. Phys. 39 (Part 1, 2A) (2000) 368–371.
[21] Koun Shirai, Temperature dependence of Young's modulus of silicon, Jpn. J. Appl. Phys. 52 (1) (2013), 088002.
[22] H. McSkimin, W. Bond, Elastic moduli of diamond, Phys. Rev. 105 (1) (1957) 116–121.
[23] H.J. McSkimin, P. Andreatch, Elastic moduli of diamond as a function of pressure and temperature, J. Appl. Phys. 43 (7) (1972) 2944–2948.
[24] P. Djemia, C. Dugautier, T. Chauveau, E. Dogheche, M. De Barros, L. Vandenbulcke, Mechanical properties of diamond films: a comparative study of polycrystalline and smooth fine-grained diamonds by Brillouin light scattering, J. Appl. Phys. 90 (8) (2001) 3771–3779.
[25] P. Djemia, A. Tallaire, J. Achard, F. Silva, A. Gicquel, Elastic properties of single crystal diamond made by CVD, Diam. Relat. Mater. 16 (4–7) (2007) 962–965.
[26] R. Vogelgesang, A.K. Ramdas, S. Rodriguez, M. Grimsditch, T.R. Anthony, Brillouin and Raman scattering in natural and isotopically controlled diamond, Phys. Rev. B Condens. Matter 54 (6) (1996) 3989–3999.
[27] J.-Å. Schweitz, Mechanical characterization of thin films by micromechanical techniques, MRS Bull. 17 (7) (1992) 34–45.
[28] H.D. Espinosa, B. Prorok, B. Peng, K. Kim, N. Moldovan, O. Auciello, J. Carlisle, D. Gruen, D. Mancini, Mechanical properties of ultrananocrystalline diamond thin films relevant to MEMS/NEMS devices, Exp. Mech. 43 (3) (2003) 256–268.
[29] N. Nakamura, H. Ogi, M. Hirao, Elastic constants of chemical-vapor-deposition diamond thin films: resonance ultrasound spectroscopy with laser-Doppler interferometry, Acta Mater. 52 (3) (2004) 765–771.
[30] C.A. Klein, G.F. Cardinale, Young's modulus and Poisson's ratio of CVD diamond, Diam. Relat. Mater. 2 (5–7) (1993) 918–923.
[31] V.P. Adiga, A.V. Sumant, S. Suresh, C. Gudeman, R.W. Carpick, Temperature dependence of mechanical stiffness and dissipation in ultrananocrystalline diamond authors, Proc. SPIE 7318 (2009) 731818.
[32] M. Núñez Valdez, K. Umemoto, R.M. Wentzcovitch, Elasticity of diamond at high pressures and temperatures, Appl. Phys. Lett. 101 (17) (2012) 171902.
[33] Z. Zhang, H. Wu, L. Sang, J. Huang, Y. Takahashi, L. Wang, M. Imura, S. Koizumi, Y. Koide, M. Liao, Single-crystal diamond microelectromechanical resonator integrating with magneto-strictive galfenol film for magnetic sensor, Carbon 152 (2019) 788–795.
[34] M. Liao, Progress in semiconductor diamond photodetectors and MEMS sensors, Funct. Diamond 1 (1) (2021) 29–46.
[35] M. Mohr, F. Picollo, A. Battiato, E. Bernardi, P. Olivero, Characterization of the recovery of mechanical properties of ion-implanted diamond after thermal annealing, Diam. Relat. Mater. 63 (7) (2015) 702–708.
[36] T. Christopoulos, O. Tsilipakos, G. Sinatkas, E.E. Kriezis, On the calculation of the quality factor in contemporary photonic resonant structures, Opt. Express 27 (10) (2019) 14505–14522.
[37] W. Weaver Jr., S.P. Timoshenko, D.H. Young, Vibration Problems in Engineering, 5th ed., John Wiley & Sons, USA, 1990.
[38] P. Singh, R. Yadava, Effect of surface stress on resonance frequency of microcantilever sensors, IEEE Sensors J. 18 (18) (2018) 7529–7536.
[39] Y.-Y. Chang, S.D. Jacobsen, M. Kimura, T. Irifune, I. Ohno, Elastic properties of transparent nano-polycrystalline diamond measured by GHz-ultrasonic interferometry and resonant sphere methods, Phys. Earth Planet. Inter. 228 (2014) 47–55.
[40] M. Grimsditch, A. Ramdas, Brillouin scattering in diamond, Phys. Rev. B 11 (8) (1975) 3139.
[41] P. Lu, F. Shen, S. O Shea, K. Lee, T. Ng, Analysis of surface effects on mechanical properties of microcantilevers, Mater. Phys. Mech. 4 (2001) 51–55.
[42] A.H. Ghadimi, S.A. Fedorov, N.J. Engelsen, M.J. Bereyhi, R. Schilling, Elastic strain engineering for ultralow mechanical dissipation, Science 360 (2018) 764–768.
[43] L. Sang, M. Liao, X. Yang, H. Sun, J. Zhang, M. Sumiya, B. Shen, Strain-enhanced high Q-factor GaN micro-electromechanical resonator, Sci. Technol. Adv. Mater. 21 (1) (2020) 515–523.
[44] H. Wu, L. Sang, Y. Li, T. Teraji, T. Li, M. Imura, J. You, Y. Koide, M. Toda, M. Liao, Reducing intrinsic energy dissipation in diamond-on-diamond mechanical resonators toward one million quality factor, Phys. Rev. Mater. 2 (9) (2018), 090601.
[45] Y. Tao, J.M. Boss, B. Moores, C.L. Degen, Single-crystal diamond nanomechanical resonators with quality factors exceeding one million, Nat. Commun. 5 (1) (2014) 1–8.
[46] H. Sun, L. Sang, H. Wu, Z. Zhang, T. Teraji, T.-F. Li, J. You, M. Toda, S. Koizumi, M. Liao, Effect of deep-defects excitation on mechanical energy dissipation of single-crystal diamond, Phys. Rev. Lett. 125 (20) (2020) 206802.

[47] T. Sato, K. Ohashi, T. Sudoh, K. Haruna, H. Maeta, Thermal expansion of a high purity synthetic diamond single crystal at low temperatures, Phys. Rev. B 65 (9) (2002) (92102-92100).
[48] J.B. Wachtman, W.E. Tefft, D.G. Lam, C.S. Apstein, Exponential temperature dependence of Young's modulus for several oxides, Phys. Rev. 122 (6) (1961) 1754–1759.
[49] William B. Hillig, A methodology for estimating the mechanical properties of oxides at high temperatures, J. Am. Ceram. Soc. 76 (1) (1993) 129–138.
[50] F. Szuecs, M. Werner, R.S. Sussmann, C.S.J. Pickles, H.J. Fecht, Temperature dependence of Young's modulus and degradation of chemical vapor deposited diamond, J. Appl. Phys. 86 (11) (1999) 6010–6017.
[51] A. Migliori, H. Ledbetter, R.G. Leisure, C. Pantea, J.B. Betts, Diamond's elastic stiffnesses from 322 K to 10 K, J. Appl. Phys. 104 (5) (2008) 101.
[52] T. Singh, M.J. Behr, E.S. Aydil, D. Maroudas, First-principles theoretical analysis of pure and hydrogenated crystalline carbon phases and nanostructures, Chem. Phys. Lett. 474 (1–3) (2009) 168–174.
[53] O.H. Nielsen, Optical phonons and elasticity of diamond at megabar stresses, Phys. Rev. B 139 (1986) 202–205.
[54] D.G. Clerc, H. Ledbetter, Second-order and third-order elastic properties of diamond: an ab initio study, J. Phys. Chem. Solids 66 (10) (2005) 1589–1597.
[55] C.J. Ruestes, A. Stukowski, Y. Tang, D.R. Tramontina, P. Erhart, B.A. Remington, H.M. Urbassek, M.A. Meyers, E.M. Bringa, Atomistic simulation of tantalum nanoindentation: effects of indenter diameter, penetration velocity, and interatomic potentials on defect mechanisms and evolution, Mater. Sci. Eng. A 613 (2014) 390–403.